Multiplexed-Based Assessment of DNA Damage Response to Chemotherapies Using Cell Imaging Cytometry

Nadia Vezzio-Vié, Marie-Alice Kong-Hap, Eve Combès, Augusto Faria Andrade, Maguy del Rio, Philippe Pasero, Charles Theillet, Céline Gongora, Philippe Pourquier

Multiplexed-based assessment of DNA damage response to chemotherapies using cell imaging cytometry

Nadia Vezzio-Vie[1], Marie-Alice Kong-Hap[1,2], Eve Combès[1], Augusto Faria Andrade[1], Maguy Del Rio[1], Philippe Pasero[2], Charles Theillet[1], Céline Gongora[1]*, Philippe Pourquier[1]*

[1]Institut de Recherche en Cancérologie de Montpellier, INSERM U1194, Université de Montpellier, Institut régional du Cancer de Montpellier, Montpellier, F-34298, France

[2]Institut de Génétique Humaine, CNRS, Université de Montpellier, Laboratoire Maintien de l'Intégrité du Génome au cours de la Réplication, Montpellier, F-34090, France

*Correspondence: philippe.pourquier@inserm.fr ; celine.gongora@inserm.fr

Tel. : +33-4-11-28-31-09

ABSTRACT

Current methods for measuring DNA damage response (DDR) are relatively labor intensive and usually based on Western blotting, flow cytometry and/or confocal immunofluorescence analyses. They require numerous cells and are often limited to a single or few proteins' assessment. Here, we used the Celigo® image cytometer to evaluate cell response to DNA-damaging agents based on a panel of biomarkers associated with the main DDR signaling pathways. We investigated the cytostatic or/and the cytotoxic effects of these drugs using simultaneous propidium iodide and calcein-AM staining. We also describe new dedicated multiplexed protocols to investigate the qualitative (phosphorylation) or the quantitative changes of 11 DDR markers on a multiplexed basis, including H2AX, DNA-PKcs, ATR, ATM, CHK1, CHK2, 53BP1, NBS1, RAD51, P53, P21. The results of our study clearly show the advantage of using this methodology as multiplexed-based evaluation of these markers can be performed in a single experiment using standard 384-well plates format. Analyses of multiple DDR markers together with cell cycle status further provide with valuable indications on the mechanism of action of investigational drugs inducing DNA damages in a

time- and cost-effective manner due to the low amounts of antibodies and reagents that are required.

Keywords : Imaging cytometry, DNA damage response, DNA repair, Biomarkers, Anticancer drugs, oxaliplatin, ATR inhibitor

INTRODUCTION

Despite the significant improvement of survival that can be obtained with immune checkpoint inhibitors, conventional chemotherapies still occupy a major place in the drug armamentarium and a large proportion of cancer patients remain confronted to treatment failures due to resistance mechanisms. This explains why there is still an active search for compounds with new mechanism of action or new synthetic lethal drug combinations that could be used as potential alternatives. The identification of a potential drug candidate that may enter clinical trials is a long and costly process that requires the validation of *in vitro* and *in vivo* studies using an increasing number of cellular and animal models to ensure its efficacy and the absence of toxicity as well as to validate its cellular target(s). A key step that is inevitable in the early preclinical development of anticancer drugs resides in the evaluation of their activity on the proliferation of cancer cells. This is usually achieved by using a wide range of cytotoxicity assays going from a simple cell count using Malassez counting chamber or automatic cell counters [1], to more sophisticated colorimetric assays indirectly measuring cell number by quantifying the total amount of proteins (ex: Sulforhodamine B assay), or measuring the cell viability by quantifying the activity of specific metabolic enzymes (ex: MTT assay and its derivatives MTS, XTT and WST, or resazurine reduction assays), or the ATP content (ex: CellTiter-Glo®, ATPLite™) (reviewed in [2]). While these assays are performed in 96-, 384-, or 1536-well plates and are particularly adapted to automation for the screening of large library of compounds, they are not giving access to much information regarding the potential mechanism of action of the drug. Flow cytometry is another method that can also be used to evaluate cell response to a cytotoxic drug, as it can distinguish between live and dead cells with the use of specific dyes that are excluded from viable cells while they penetrate into damaged cells. Propidium iodide is a well-known example to illustrate that point as it is extensively used to discriminate dead cells, that are permeable to this dye regardless of the mechanism of death, from live cells with intact membranes [3]. Though it is accurate, flow cytometry requires a relatively high number of cells, robust controls, and specific skills to operate and maintain instrumentation platforms on a routine basis [4]. Another important limitation of these methodologies is the absence of cell visualization that may bias the interpretations of the results.

In the past decades, several companies have developed automated plate-based cell imaging cytometers such as the Celigo® (Nexcelom Bioscience) [5], Opera (Perkin Elmer) [6], IN Cell Analyzer 2200 (GE) [7], Spark® Cyto (Tecan) [8], CELLAVISTA® 4 or

NYONE® (Synentec) [9,10], Cytation 5 (Biotek) [11], SpectraMax MiniMax 300 (Vertex) [12], or CellInsight CX series (ThermoFisher Scientific) [13,14], or ImageXpress PICO (Molecular Devices) [15]. These cytometers were developed to analyze cell survival by simultaneously evaluating live and dead cells and also various targets of interest within the same cells as long as these targets could be fluorescently stained, thereby reducing the number of manipulations that could affect the robustness of the assay. These platforms are particularly adapted for the assessment of the phosphorylation status of key proteins involved in various signaling pathways that may play a role in cancer cell proliferation or cell response to anticancer drugs.

In this study we have used the Celigo® platform to study the effects of a panel of chemotherapies on both cell proliferation and cell death. This allows to rapidly identify the cytotoxic or the cytostatic nature of the tested drugs and the contribution of each mechanism to cell growth inhibition. We also provide the experimental conditions to study the cell response to these chemotherapies that directly target DNA or that induce replicative stress ultimately leading to lethal DNA double-strand breaks by analyzing, on a multiplexed basis, the qualitative (phosphorylation status) and the quantitative changes (number of labeled cells and their intensity of labeling) of various DDR markers within the same cells, including H2AX, DNA-PKcs, ATR, ATM, CHK1, CHK2, 53BP1, NBS1, RAD51, P53, P21. Interestingly activation of these DDR markers could be identified in cells depending on their cell cycle status, which is also an advantage of this methodology. The results of our study clearly show a heterogeneity of cell response to DNA damaging agents within the same population, which cannot be assessed by Western blotting. We could validate this methodology by testing the synergistic combination of oxaliplatin and the ATR inhibitor VE-822 and confirmed that VE-822 could enhance replicative stress and increase lethal DNA double-strand breaks [16]. This study is providing with a first set of methodological protocols for the use of the Celigo® image cytometer to study the mechanism of DDR response to investigational drugs. They will serve as a basis for the development of new pertinent sets of markers involved in DNA damage signaling.

RESULTS

1. Dual evaluation of cytotoxic and cytostatic effects of antiproliferative agents using image cytometry

The evaluation of the cytotoxic potential of any compound is usually the first step in the preclinical development of anticancer drugs. It is usually evaluated using high throughput screens in cancer cell lines where the effect of the drugs on either cell viability or cell death are measured. These in vitro assays are performed in multi-well plates in which a global quantification of living cells or dead cells in each well is obtained using colorimetric assays or fluorescence- or luminescence-based protocols. While these assays could give a relatively frank account on the activity of a drug, they usually measure a single parameter.

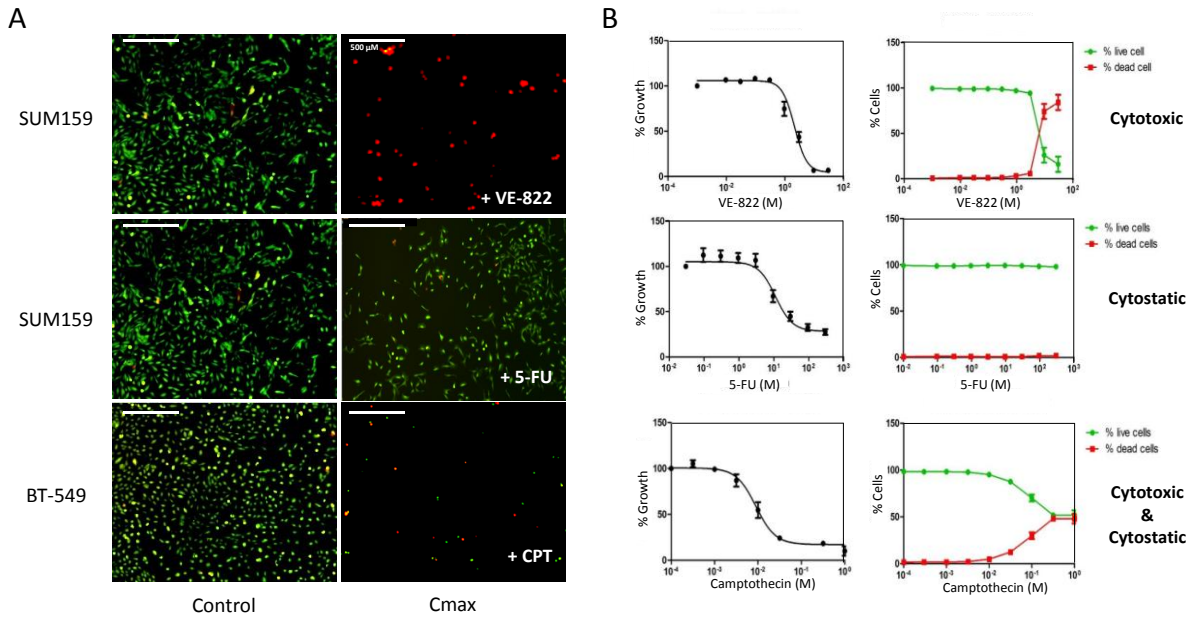

Figure 1. Dual assessment of the cytotoxic and the cytostatic effects of drugs using the Celigo® imaging cytometer. **(A)** Triple negative breast cancer cells, SUM159 and BT-549, were treated with increasing concentration of each drug for 72 h. Then, dual staining with propidium iodide (PI) and calcein AM was performed to respectively visualize dead cells (red) and live cells (green) within each well. **(B)** Quantitation of the results obtained in panel (A) using the dedicated Celigo® software. Right panels show the percentages of dead cells and live cells relative to untreated controls as a function of drug concentrations. Left panels: Total cell number (live + dead cells) in each well was calculated and normalized to untreated controls and percentages were plotted as a function of drug concentrations to evaluate IC_{50} values. Results are the mean ± SEM of ≥ 3 independent experiments.

Using image cytometry, we used established protocols to evaluate the effect of anticancer drugs on the number of cells and on both cell viability and cell death within the same population (Fig. 1, Table 1).

For this purpose, a panel of cancer cell lines from breast, prostate and ovarian origin were seeded in 96-well plates and treated for 72 h with increasing concentrations of several cytotoxic agents that are known to induce DNA damage. In most cases, cells were labelled with propidium iodide and calcein-AM without removing supernatants to respectively visualize dead cells and live cells in each well prior to image acquisition (Fig. 1A). Using a dedicated software, cell contouring was then performed based on each fluorescent labelling. One should notice that when cell shape and/or cell density precluded adequate cell contouring for calcein-AM-stained cells, nuclear staining with Hoechst was used. Representative images of PI (red) and Hoechst (blue) dual staining for OVSAHO and DU145 cells treated respectively with cisplatin and camptothecin are shown as an example (Fig. S1).

Image analyses allowed to get access to the percentages of dead and live cells per well that were further plotted as a function of drug concentrations (Fig. 1B, right panel). Percentages of growth inhibition could also be calculated based on the total number of cells (live + dead) in each well as compared to untreated controls and plotted as a function of drug concentrations to evaluate IC_{50} values (concentration of the drug that inhibits 50% of cell growth) (Fig. 1B, left panel). The results of figure 1B illustrates the three main categories of effects that can be observed: drugs that are mainly cytotoxic such as VE-822 in SUM159 cells; drugs that are primarily cytostatic such as 5-FU in SUM159 cells; and drugs that exert both cytostatic and cytotoxic effects such as camptothecin in BT-549 cells.

We also show that depending on the cell line, the effect of a drug on growth inhibition may not result from the same mechanism of action. Indeed, at a concentration of 0.1 µM that inhibited the growth of all cell lines tested by ~80% (Fig. S2A), camptothecin was mainly cytostatic in OVSAHO cells (less than 10% of dead cells), whereas it was primarily cytotoxic in HCC38 cells with a percentage of dead cells that reached 80% and displayed both cytostatic and cytotoxic effects in DU145 and PC3 cells (Fig. S2B).

Using imaging cytometry, it is then possible to rapidly get access, in a single experiment, to the IC_{50} values of several drugs as well as a quantitative assessment of both the cytostatic and the cytotoxic effects that are involved (Fig. 1). Table 1 recapitulates data for 9 different cancer cell lines and 9 different drugs leading to a color-coded classification that

indicates the contribution of each type of mechanism. It is interesting to note that, regardless of the cell line, some drugs are mainly cytostatic as it is the case for 5-FU, olaparib and oxaliplatin to a lower extent. On the contrary, decrease in cell numbers induced by camptothecin and VE-822 is mainly due to a cytotoxic effect. Our screen also revealed differential sensitivity to DNA damage depending on the cell line, breast cancer cell lines (and especially HCC38 cells) being globally more sensitive to DNA damaging agents than prostate or ovarian cancer cell lines (Table 1).

	Breast				Ovarian		Prostate		
	BT-549	SUM159	HCC38	MDA-MB-436	OVSAHO	OVCAR-8	DU 145	PC-3	22Rv1
Camptothecin	0.012 ± 0.005	0.008 ± 0.002	0.0078 ± 0.0037	0.01 ± 0.003	0.0093 ± 0.0006	0.0047 ± 0.0006	0.013 ± 0.003	0.012 ± 0.002	0.0185 ± 0.006
Cisplatin	1.33 ± 0.58	3.5 ± 2.5	4 ± 2.4	0.47 ± 0.16	2.75 ± 1.26	1.24 ± 0.31	1.6 ± 0.26	1.17 ± 0.40	2.43 ± 0.51
Etoposide	1.35 ± 1.05	0.37 ± 0.06	0.48 ± 0.22	0.16 ± 0.03	1.03 ± 0.45	0.46 ± 0.21	0.155 ± 0.013	n.d.	0.25 ± 0.06
5-FU	> 100	33 ± 12.0	> 100	9 ± 1	83.3 ± 28.8	8.33 ± 1.53	6 ± 3	13 ± 8.9	16 ± 2
Gemcitabine	0.007 ± 0.001	0.008 ± 0.004	0.0065 ± 0.003	0.006 ± 0.002	0.0087 ± 0.0011	0.004 ± 0.001	0.00325 ± 0.0006	0.008 ± 0.04	0.008 ± 0.0006
Olaparib	> 100	22.8 ± 6.5	5.5 ± 2.6	2.4 ± 1.1	> 100	7.7 ± 2.1	4.375 ± 1.25	n.d.	14.25 ± 7.63
Oxaliplatin	1.5 ± 0.5	4.7 ± 2.3	4.3 ± 2.5	5.7 ± 4.04	4.7 ± 1.5	2.83 ± 0.15	3.0 ± 0.006	2.5 ± 0.26	4.83 ± 2.25
PF477736	1.17 ± 0.35	1.77 ± 0.87	0.027 ± 0.003	0.027 ± 0.004	0.9 ± 0.21	0.23 ± 0.025	0.0825 ± 0.005	0.54 ± 0.37	0.08 ± 0.02
VE822	0.68 ± 0.36	1.86 ± 0.9	0.23 ± 0.03	0.58 ± 0.24	1.5 ± 0.5	1.08 ± 0.03	0.725 ± 0.29	1.37 ± 0.25	1.95 ± 0.9

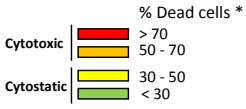

Table 1. Effects of DNA damaging agents on growth inhibition in various human cancer cell lines. Cells were treated with increasing concentrations of each drug for 72h continuously and processed as in figure 1. Each value corresponds to the IC_{50} concentration (in µM) (concentration inhibiting cell growth by 50%) ± SD of 3 independent experiments. The color code corresponds to the effects (cytostatic or cytotoxic) of each compound contributing to growth inhibition; green: primarily cytostatic, yellow: cytostatic ≥ cytotoxic orange: cytostatic ≤ cytotoxic, red: mainly cytotoxic. Drugs mechanism of action: camptothecin: DNA topoisomerase I inhibitor; etoposide: DNA topoisomerase II inhibitor; cisplatin & oxaliplatin: DNA crosslinking agents; gemcitabine: DNA chain terminator; 5-FU: antimetabolite; Olaparib: PARP inhibitor; PF477736: Chk1 inhibitor; VE822: ATR inhibitor

2. Image cytometry for the evaluation of DDR using γH2AX as a marker

We then established a quantitative immunofluorescence assay to assess the DNA damage response to commonly used anticancer agents. For this purpose, we used black-sided, flat-bottomed 384-well plates that allow to screen in a single run the effects of two drugs at 5 concentrations on up to 8 DDR markers in triplicate. Cells were seeded at their optimal density and were treated with the tested drugs 24 hours later. Cells were then fixed and permeabilized directly in the well without trypsinization hence preserving the phosphorylation status of the DDR markers. Immunostaining was then performed with the specific antibodies according to the protocol that is outlined in the flow chart of Figure 2A.

To standardise each experiment, we used a positive control where cells were treated with a high concentration of the Top1 inhibitor SN38 (2 µM) in order to set dye exposures. To assess the background noise, we used untreated cells only stained with the secondary antibody (CT). First, experimental settings were established to evaluate the DDR of HCT116 colon cancer cells to SN38 using γH2AX as a DDR marker (Fig. 2B).

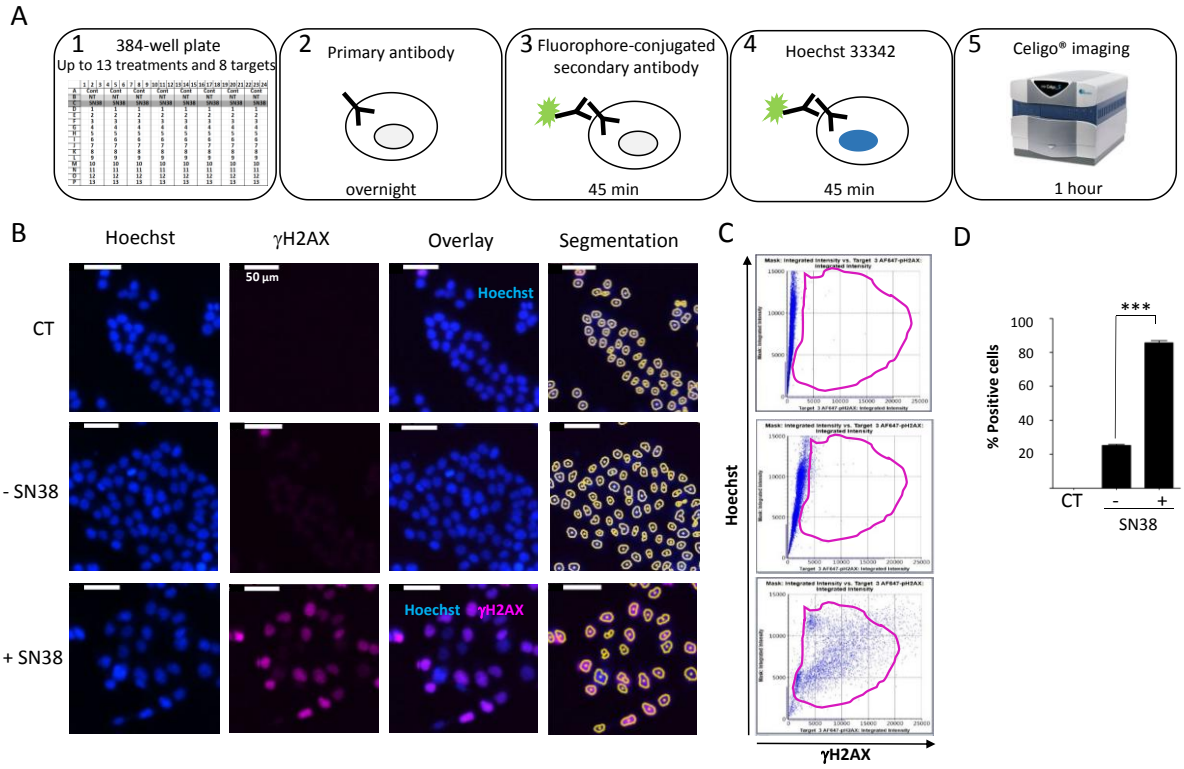

Figure 2. (A) Celigo® imaging flow chart used for DDR evaluation. **(B)** Representative fluorescence images of H2AX phosphorylation obtained for HCT116 cells in the absence or in the presence of SN38 (2 µM, 24 h). Hoechst was used for nuclear staining and total cell count using the dedicated segmentation protocol (right panel). Images were acquired and analysed using the Target + Mask application. CT: control cells stained with the secondary antibody alone. **(C)** Representative flow-like analyses of the images obtained in (B). The dot-plots show Hoechst integrated intensity as a function of γH2AX integrated intensity. A gate (in purple) was defined for the control condition (CT) and applied to all other conditions to determine the percentage of positive cells and the fluorescence intensity in each cell. **(D)** Percentages of fluorescent positive cells for γH2AX labelling are plotted as a function of cell treatment. The bar graphs represent the quantitative analyses (mean ± SD ; n=3) of the fluorescent images from one representative experiment. Statistical analysis was carried out using Student's *t*-test; (***): $p<0.0001$.

Staining with Hoechst was performed concomitantly to enable cell segmentation. The mask that was obtained was applied to each well to quantify each fluorescence signals in individual nuclei. Representative images were subsequently analysed using the dedicated software. Analysis steps (Hoechst vs γH2AX) were similar to standard flow cytometry analyses (Fig. 2C). A gate was then generated based on the background staining (CT) and applied to each condition. Using these settings, it is possible to get access to both the number of fluorescent cells in each channel following drug treatment and to the average integrated intensity of the fluorescence per cell. The results of our set-up experiment confirmed that SN38-mediated DNA damage is inducing the phosphorylation of H2AX, as evidenced by the significant increase in the percentage fluorescent cells as compared to controls (Fig. 2D). These results further validate the use of image cytometry to rapidly and quantitatively assess DDR to various antiproliferative agents in a multiplexed manner.

3. Evaluation of other DDR markers

We then extended our study to an additional panel of 11 DDR markers based on their reported key role in DNA damage signalling and/or repair, including H2AX, DNA-PKcs, ATR, ATM, CHK1, CHK2, 53BP1, NBS1, RAD51, P53 and P21, most of them being phosphorylated following DNA damage.

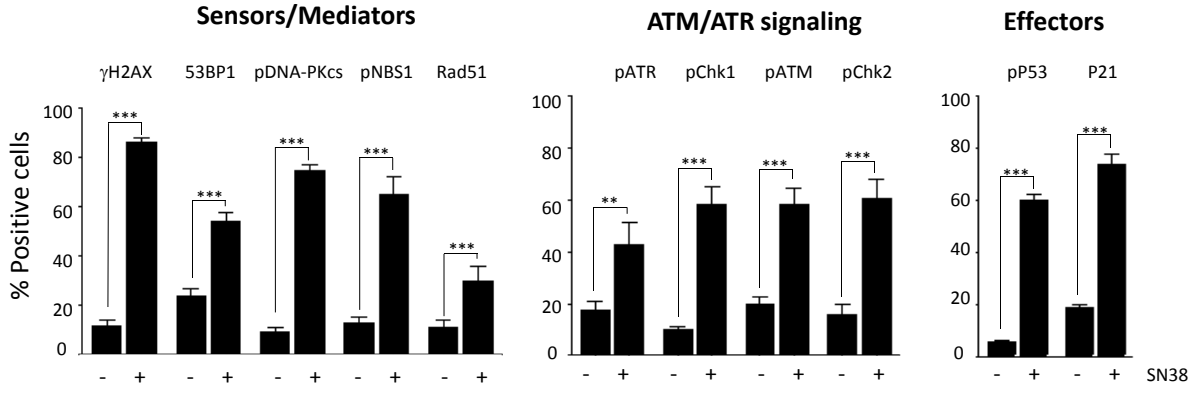

Figure 3. Monitoring of HCT116 cell response to SN38 using a panel of DDR markers. Cells were treated with 2 µM SN38 for 24h and immunofluorescence staining was performed with antibodies targeting γH2AX, 53BP1, phospho-NBS1, Rad51, phospho-DNA-PKcs, phospho-ATR, phospho-Chk1, phospho-ATM, phospho-Chk2, phospho-P53, P21 as indicated in Materials and Methods. Quantification of fluorescent positive cells were determined for each DDR marker in untreated cells and cells treated with SN38. Results are the mean ± SEM of ≥

3 independent experiments. Statistical analysis was carried out using Student's *t*-test and considered statistically significant for $p<0.01$ (**), and $p<0.001$ (***), respectively.

Antibodies were selected based on their specificity and their suitability for immunofluorescence application as indicated in the manufacturers' documentations (Table S1). We first identified the optimal experimental conditions for each DDR marker following treatment with SN38, in particular the antibodies' dilutions (Fig. S3). Quantitation of DDR was then performed as described for γH2AX and percentages of fluorescent-positive cells (Fig. 3) were determined for each marker in SN38-treated HCT116 cells. As expected, the results show a significant increase in the number of fluorescent cells for all DDR markers that were analyzed, confirming that SN38 induces the activation of both the ATR/CHK1 and ATM/CHK2 pathways, as DNA topoisomerase I poisons are known to generate both single- and double-strand DNA breaks [17]. We also evidenced an increase in the number of cells with phosphorylated P53 (Ser 15) and P21, in line of what have been reported previously [18]. In most cases, the increase in the percentage of fluorescent cells was accompanied with a significant increase in the average fluorescence intensity (data not shown).

We then extended our analyses to compare the effects of SN38 to three other DNA damaging agents with different mechanisms of action: etoposide (ETO), hydroxyurea (HU) and oxaliplatin (OX) (Fig. 4). Using the same experimental set up, we performed dose-response experiments and measured the changes in the phosphorylation of DDR markers. The number of fluorescent-positive cells was then quantified for each marker as previously described. The results were expressed as fold changes as compared to untreated cells to allow a comparison between drugs as basal level of fluorescence and induction of phosphorylation was not similar depending on the drug and on the DDR marker. An increase in the number of fluorescent-positive cells was observed in most cases and it was generally concentration-dependent (Fig. 4). The extent of that increase was however quite variable depending on the marker and on the drug used. As an example, the number of cells with phosphorylated DNA-PKcs following SN38 or etoposide treatment was increased by ~20-fold for concentrations inducing > 75% growth inhibition (Fig. S4), whereas increase was limited to ~2-fold for oxaliplatin treatment (Fig. 4).

In the case of 53BP1, increase in the number of fluorescent positive cells was marginal as it never exceeded 2-fold regardless of the drug and of the concentrations used. The effects of duration of treatment on the status of DDR markers were also evaluated by quantifying the

percentages of γH2AX, phospho-CHK1 and phopsho-CHK2 fluorescent-positive cells at 5h and 20h time points (Fig. S5).

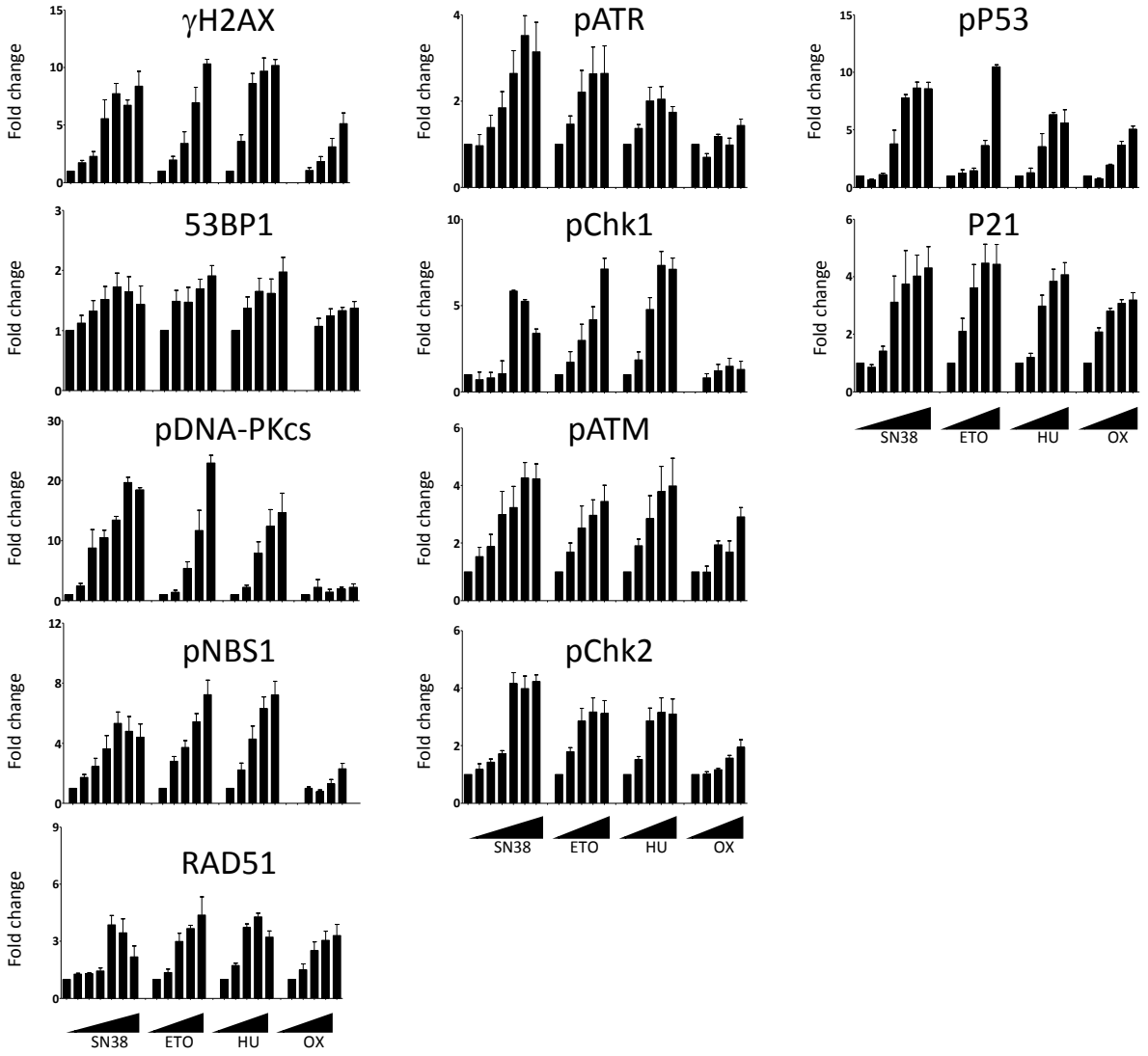

Figure 4. Dose-dependent DDR response of HCT116 cells to DNA damaging agents. Cells were treated overnight with increasing concentrations of SN38 (0, 0.2, 1, 5, 16, 80, 2000 nM), Etoposide (0, 1, 2, 6, 30, 150 µM), Hydroxyurea (0, 0.12, 0.6, 3, 15 mM), or Oxaliplatin (0, 0.4, 2, 10, 50 µM) and DDR markers were evaluated as indicated in figure 3. The results show the ratios of the average number of fluorescent cells following SN38 treatment as compared to untreated cells for each DDR marker. Results are the mean ± SEM of 2-4 independent experiments.

As anticipated, the number of fluorescent-positive cells was generally lower when cells were treated for 5h as compared to cells treated for 20h, with the exception of oxaliplatin for which increase in the percentage of phosphorylated H2AX was more pronounced at 5h

than at 20h suggesting different kinetics or DNA break formation/repair for this platinum derivative (Fig. S5). This is also the case for hydroxyurea (HU), an inhibitor of the ribonucleotide reductase that blocks DNA replication by depleting the pool of DNA precursors via the inhibition of the ribonucleotide reductase [32]. HU induces replication fork stalling and S-phase arrest that further lead to DNA damage including DSBs [33]. We showed that DNA damage signaling was not detected after a 5 h treatment whereas H2AX phosphorylation was significantly enhanced following a 20 h treatment with HU, suggesting that drugs acting on nucleotide synthesis may require longer duration of treatment for testing.

4. Cell cycle-specific analysis of DDR markers

Another interesting feature of the Celigo® image cytometer is the possibility to have access to the cell cycle distribution concomitantly to the DDR marker status within the same cell population, thanks to Hoechst staining that was used for both cell count and determination of the DNA content (Fig. 5). HCT116 cells were treated with etoposide (100 µM, 20h). γH2AX and Hoechst staining were performed concomitantly as previously described. A significant increase in the number of fluorescent cells with phosphorylated H2AX was observed in etoposide-treated cells which confirmed various studies (Fig. 5A). Hoechst integrated intensity could be visualized as a histogram plot showing the cell cycle distribution within the cell population (Fig. 5B).

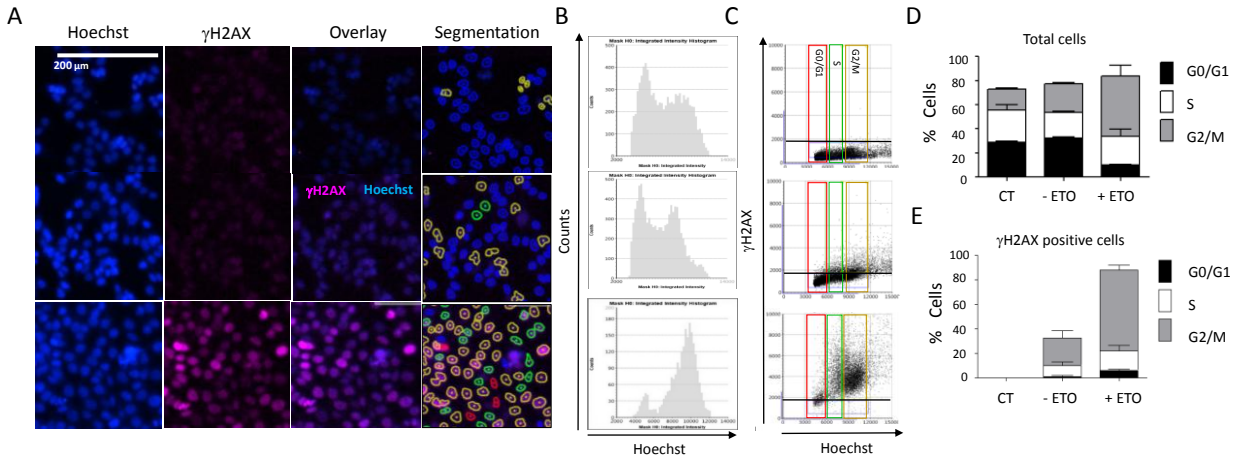

Figure 5. DDR response and cell cycle analyses. **(A)** HCT116 cells were treated with 100 µM Etoposide for 20h. Cells were then fixed and stained for DNA with Hoechst and for γH2AX and plates were analysed using the Celigo® as described in figure 3. Representative fluorescence images are shown for each condition. Hoechst staining was used for segmentation and to quantify the DNA content in each cell. **(B)** Cell cycle profiles showing

total cells' distribution depending on their DNA content as evaluated by the Celigo® flow cytometry interface. **(C)** Distribution of γH2AX-positive cells depending on their cell cycle phase as determined by the segmentation process according to the following colour code: red: G0/G1, green: S, brown: G2/M. **(D, E)** Quantitation of the results shown in (B) and (C), respectively. Three independent experiments have been performed. Results are the mean ± SD of a technical triplicate from one representative experiment. CT: untreated cells stained with the secondary antibody alone.

Image analyses showed that etoposide treatment induced a G2/M accumulation (Fig 5B & 5C) with a percentage of cells blocked in this phase reaching 66% as compared to 22% for the untreated control (Fig. 5D). This was consistent with the results that were obtained when percentages of H2AX positive cells were quantified in each phase of the cell cycle (Fig. 5E). Using image cytometry, it is therefore possible to follow the change in DDR marker within each cell of the population, but also to indicate the cell cycle phase in which such a change has occurred, which provides precious indications on the mechanism of the tested drugs.

5. Multiplexed analyses

Because the Celigo® image cytometer can be equipped with 4 LED-based fluorescent channels allowing multiplexed analyses of up to three DDR markers together with Hoechst nuclear staining. As an example, we analyzed HCT116 cells treated with SN38 (2 µM, 24h) and a concomitant labeling of two downstream effectors of DNA damage signaling, pP53 and P21, together with Hoechst (Fig. 6A). Prior to the experiment, conditions for DDR marker multiplexing were optimized for each marker individually to validate the absence of overlap of the fluorescence signals in each channel, as illustrated in the flow-like image analyses of obtained images (Fig. S6A). Using these settings, the results show that percentages of pP53+, P21+ and pP53+/P21+ fluorescent cells were relatively low in untreated conditions (7%, 4.5%, and 10.2%, respectively) (Fig. 6A). Treatment with SN38 showed a ~2-fold increase in the percentages of cells that were positive for a single marker (7.0% to 14.1% for pP53, and 4.5% to 10.4% for P21, respectively) and an increase of ~5-fold (10.2% vs 53.8%) in the percentage of cells that were fluorescent for both pP53 and P21, which represented the majority of total fluorescent cells (Fig. 6B & S6B). Of note, a net increase in the average intensity was concomitantly observed in pP53+/P21+ fluorescent cells (Fig. 6A). These results not only confirm our previous analyses using each marker used individually (Fig. 3), but also demonstrate the interest of using multiplexed labeling as it allows the identification

of cell populations with either single- or double-fluorescent labeling that are specifically enhanced by the treatment.

Multiplexed analyses were then extended to 3 DDR markers that are known as early response markers of DNA damage signaling: γH2AX, pATM and pATR. HCT116 cells were treated with SN38 (2 µM, 24h) and staining with the pool of antibodies and Hoechst was performed according to experimental settings that were also validated following flow-like analyses of the fluorescent images that were obtained (Fig. S7).

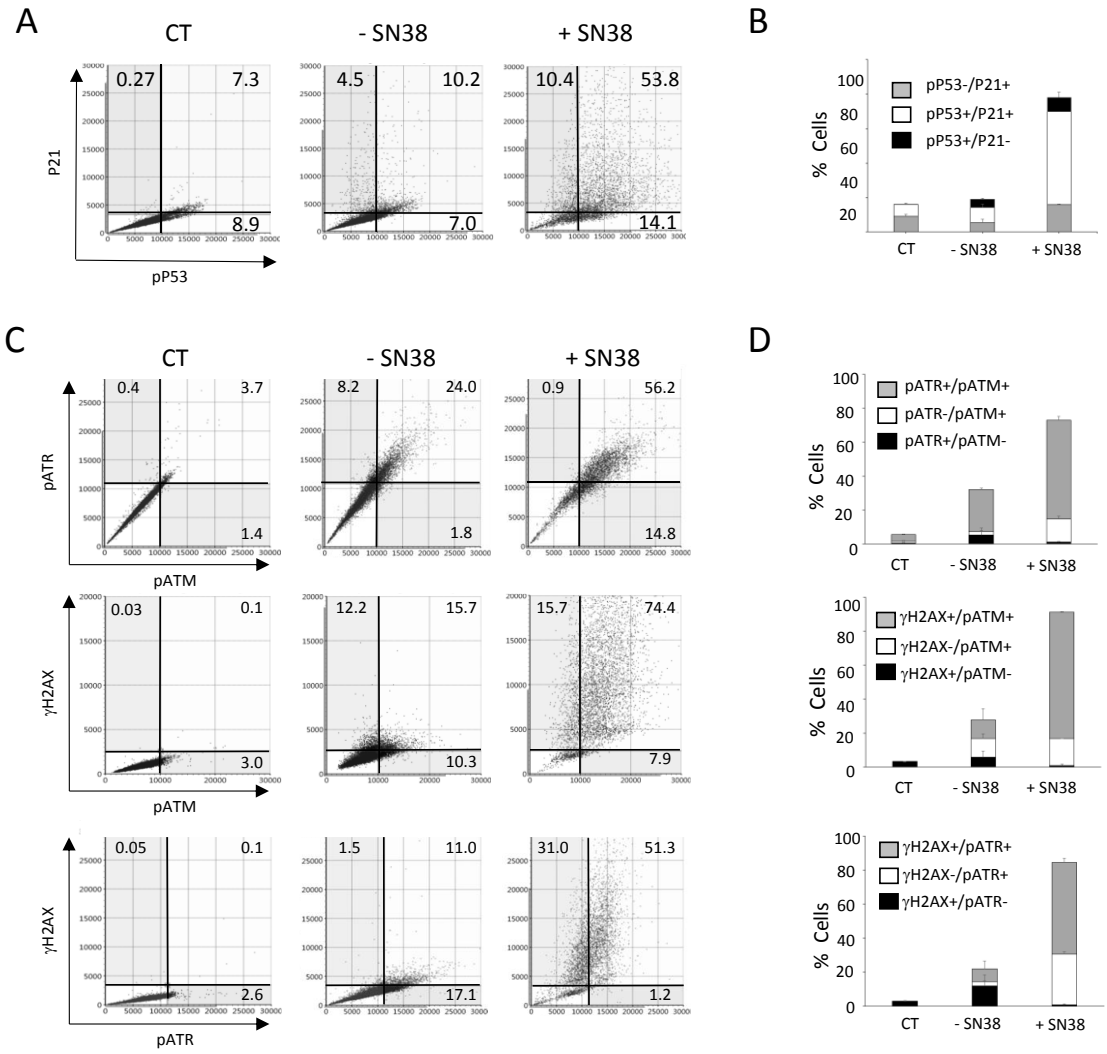

Figure 6. Multiplexed analyses of DDR markers following DNA damage. HCT116 cells were treated with SN38 (2 µM) for 20h and multiplexed immunofluorescence labelling with pATM, pATR and γH2AX or pP53 and P21 antibodies were performed and analysed using the Celigo® flow cytometry interface using a gating that was determined for the CT condition (untreated cells stained with the secondary antibody alone). **(A)** Representative dot-plots show the distribution of florescent cells depending on their DDR marker status. **(B)** Quantitation of the results shown in (A). Independent experiments have been performed twice for pATM/pATR/γH2AX labelling and three times for P21/pP53 labelling. Results are the mean ± SD of a technical triplicate from one representative experiment.

The results showed that in untreated cells (-SN38), the percentages of γH2AX-, pATR- and pATM-positive cells for a single or for two markers reached ~25% (Fig. 6C & D), which is compatible with our former analyses that were performed with each marker alone (Fig. 3). Treatment with SN38 led to a global increase in the phosphorylation of the three DDR markers leading to a global percentage of fluorescent cells that reached 90% for γH2AX, 80% for pATM and 60% for pATR (Fig. 6C & D). Our multiplexed analyses also show that the majority of the cells in which ATM or ATR were phosphorylated were also positive for γH2AX labeling with a percentage of γH2AX+/pATR+ and γH2AX+/pATM+ cells that was increased by ~5-fold following SN38 treatment (11% vs 51.3% and 15.7% vs 74.4%, respectively) (Fig. 6C & D). Thus, we could confirm that HCT116 treatment with SN38 could produce DNA damage as evidenced by the phosphorylation of both ATM and ATR leading to the phosphorylation of H2AX labeling and subsequent activation of both the ATM/CHK2 and ATR/CHK1 signaling pathways, as formerly shown (Fig. 3). These results further demonstrate that image cytometry could identify subpopulation of cells in which DDR markers are phosphorylated concomitantly following treatment with the tested drug and orient towards its mechanism of action and/or resistance.

6. Validation of the multiplexed approach using the VE-822 + Oxaliplatin (VOX) combination

We next applied our multiplexed protocol to the VOX combination, which associates the platinum salt oxaliplatin and the ATR inhibitor VE-822. Using *in vitro* and *in vivo* colon cancer cell models, we previously demonstrated that ATR inhibition by VE-822 enhanced the cytotoxicity of oxaliplatin and could potentiate the formation of DNA single- and double-strand breaks leading to apoptosis [16]. Using standard Western blots, we previously showed that, in comparison with untreated cells, treatment with VOX led to enhanced phosphorylation of several DDR markers including ATM (Ser 1981), CHK2 (Thr68), and P53 (Ser 15), which were increased by 6-fold, 12-fold and 20-fold, respectively [16]. On the contrary, a modest increase in the phosphorylation of ATR (Thr1989) and CHK1 (Ser 345) was noticed (1.2-fold and 1.9-fold, respectively) [16]. Activation of these DDR markers was observed for oxaliplatin alone and was significantly amplified by the addition of VE-822 only in the case of pATM, pCHK2 and pP53, indicating that the synergistic effect of VOX was mainly

associated with the triggering of the ATM/CHK2 pathway [16]. These results were confirmed by image cytometry analyses of each DDR marker used individually (Fig. S8).

Multiplexed analyses using γH2AX/pATM/pATR antibody combinations were also performed using the experimental conditions described earlier (Fig. 7 & 8). As compared to untreated cells, the results showed an increase in the percentage of cells that were fluorescent for γH2AX, pATM and pATR following treatment with oxaliplatin: 19% vs 1.9%, 46% vs 10%, and 55% vs 26%, respectively (Fig. 7B & 8B). As expected, addition of VE-822 to oxaliplatin led to a drastic increase of the percentage of γH2AX-fluorescent cells that reached 55% which is in accordance with the synergistic effect of the combination (Fig. 7B & 8B). Conversely, VOX treatment did not result in a significant change in the percentages of cells that were positively labelled for pATM and pATR. Our multiplexed analyses also revealed that the majority of HCT116 cells that were positively stained for pATR and pATM were also positive for γH2AX staining (Fig. 7).

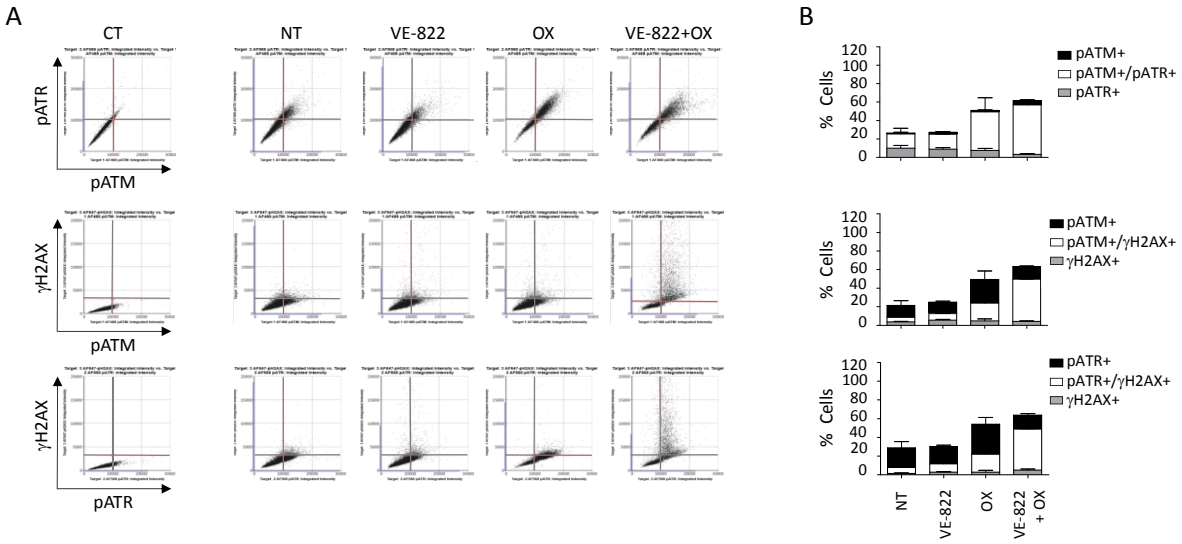

Figure 7. Multiplexed analyses of DDR markers using the VOX combination. HCT116 cells were treated with the VE-822 (1 µM), oxaliplatin (2.5 µM) or the combination of both for 24 h and DDR markers were analysed as described in figure 6. **(A)** Representative dot plots showing the distribution of fluorescent cells depending on their DDR marker status. **(B)** Quantification of fluorescent positive cells was performed for each DDR marker in untreated cells and cells treated with VE-822, OX, or the combination of both. Three independent experiments have been performed. Results are the mean ± SD of a technical triplicate from one representative experiment.

Interestingly, when cells were treated with VOX, cell-cycle analyses revealed a nearly complete abrogation of S-phase and showed that pATM, pATR and γH2AX fluorescent cells

accumulated in the G2/M phase of the cell cycle (Fig. 8). These results also revealed that, as compared to untreated cells, a significant proportion of the cell population (~40%) did not show any fluorescent staining following treatment with oxaliplatin or VOX (Fig. 7B & 8B), indicating a heterogeneity in cell response to these treatments that could not be evidenced by standard Western blotting.

Together, these results confirmed the synergistic effect of VOX that was previously observed in oxaliplatin-resistant HCT116-R1 cells [16]. VOX induced an almost complete S-phase abrogation that was accompanied with an accumulation of cells in G2/M, which is consistent with the ATR role in S and G2/M checkpoint and the repair of DNA breaks in G2 by homologous recombination [19].

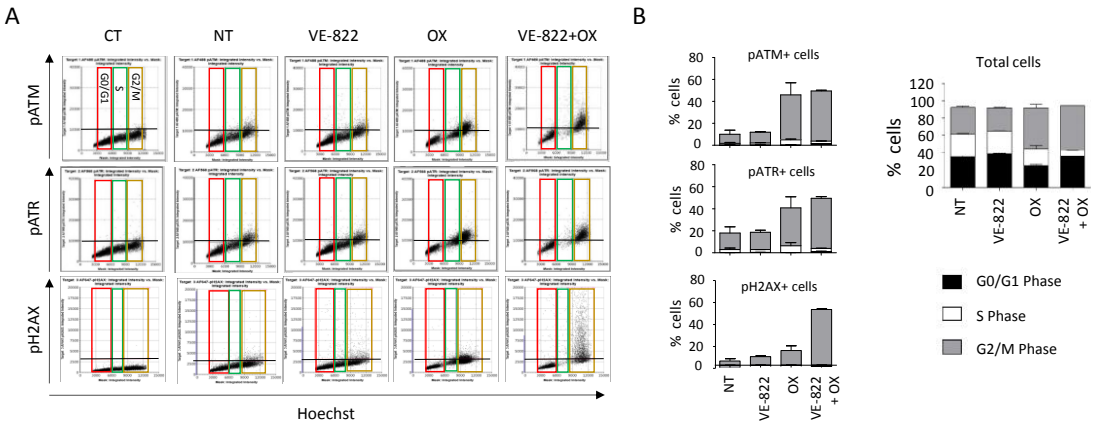

Figure 8. DDR markers analyses depending on cell cycle status following treatment with the VOX combination. HCT116 cells were treated as in figure 7 and cells' distribution depending on their DNA content and each DDR marker was obtained using the Celigo® flow cytometry interface. **(A)** Representative dot-plots obtained for each DDR marker. **(B)** Distribution of total cells and of cells positive for each DDR marker depending on their cell cycle phase. Three independent experiments have been performed. Results are the mean ± SD of a technical triplicate from one representative experiment. Coloured boxes indicate each phase of the cell cycle. red: G0/G1, green: S, brown: G2/M.

Thus, using the Celigo® image cytometer, we could set up adapted protocols to study in a short time frame the DNA damage response to a series of anticancer drugs using a panel of key DDR markers. We highlighted the possibility to monitor the activation of these markers in each phase of the cell cycle, providing additional insights on the mechanism of action of the tested drugs. Our results also emphasized the advantage to use this kind of

multiplexed approach in terms of reduced cell numbers, as well as quantities of antibodies and reagents that are necessary, leading to sizeable cost and time savings.

DISCUSSION

The initial step in preclinical development of anticancer drugs resides in the evaluation of their antiproliferative activity. This is usually achieved using a wide range of cytotoxicity assays that can be performed in 96-, 384-, or even 1536-well plates in a fully automated way, allowing for the screening of large libraries of more than hundred thousand of compounds. These campaigns have led to the identification of quite a number of hits, as in the case of the public NCI60 anticancer drug screen program using a panel of 60 cancer cell lines [20]. However, these kinds of studies were limited by the lack of information regarding the potential mechanism of action of the identified hits. Though flow cytometry-based assays can be used to assess the effects of drugs on viability or cell growth and the activation (phosphorylation) of potential targets, a major limitation resides in the absence of cell visualization that may limit the interpretations of the results as far as morphologic cell features or subcellular localization of fluorescent markers are concerned [4].

Here, we used image cytometry as an alternative to get around this limitation and chose to work with the Celigo® image cytometer, which is particularly suitable for high throughput screens because it fits standard multi-well plate formats. It beneficiates from an f-theta lens coupled with a galvanometer to provide a flat field allowing the analyses of the entire well surface [21]. With its 4 LED-based fluorescent channels it is also well adapted to multiplex labeling as it can assess up to three markers of interest together with nuclear or cytoplasm staining used for cell segmentation. We confirmed the advantages of using this platform for the high throughput evaluation of the effect of drugs on cell viability, using two combinations of dyes that could discriminate between dead and live cells, as previously reported [22]. However, we found that cytoplasmic calcein-AM staining could not be used for adherent cells with heterogenous shapes or sizes, or cells growing in clusters like OVSAHO and DU145 cells, as these characteristics deeply impaired the automatic segmentation process [23]. As an alternative, we used Hoechst nucleus staining which allowed to monitor all the cells in each well. We determined the effects of 9 anticancer drugs on the viability of 9 cancer cell lines, defining three main categories of drugs depending on whether growth inhibition was due to either a cytostatic effect, or to a cytotoxic effect or both effects. While increasing drug concentration was often correlated with increased cytotoxicity, some drugs such as 5-FU that exerts its activity through inhibition of thymidylate synthase (TS) and incorporation of its metabolites into RNA and DNA [24] was systematically cytostatic. On the contrary,

camptothecin, cisplatin, etoposide or VE-822 showed a more pronounced cytotoxic effect across our cell panel as they induced ≥ 50% cell death at concentrations that are closed to IC_{50} values. Our results also showed that the balance between the cytostatic and the cytotoxic effect of drugs was dependent on the cell model, suggesting that different signaling pathways of drug-induced DNA damages were triggered, probably due to the heterogeneity of the genomic background of these models, especially concerning DDR genes status. Table I is providing the reader with this information together with the IC_{50} values of the 9 drugs that were tested in our cancer cell panel. These drugs with known targets and mechanism of action could thus be used as a reference for further comparison with investigational drugs. It is also interesting to note that using this approach, Kuksin *et al*. were able to demonstrate the similar efficiency of image cytometry as compared to flow cytometry, with the advantage of excluding cellular debris that are often difficult to eliminate from gated cell populations [4].

Investigating the effects of DNA damage induced by genotoxic drugs is also crucial for the development of new potential anticancer agents. In this line, the detection and the quantification of DNA double-strand breaks are of particular importance as they are usually associated with the lethal effect of these molecules [25–29]. Numerous studies have proposed experimental protocols using single-cell image analyses with fluorescence microscopy to quantify DNA damage using γH2AX [30], RPA/Rad51 [31] or NBs1/Rad51 [32] foci as a biomarker. This methodology remains the most sensitive one for the quantitative and qualitative assessment of these foci, but requires the use of glass coverslips and high-resolution microscopes, that only reached semi-automated analysis. Flow cytometry was used as an alternative to reach a high-throughput scale, usually with the detection and the quantification of a single marker such as γH2AX foci to directly assess DNA double strand breaks [30], or RPA foci to quantify DNA ends' resection and DNA repair by homologous recombination [33]. In order to facilitate the detection of these markers bound to the chromatin, an extraction step was required to remove unbound proteins [34]. Though it is reliable, flow cytometry requires a large number of cells and the need to detach cells from their support before analyses. It also requires specific training to operate these platforms on a routine basis and is usually associated with high maintenance costs.

In this study we used image cytometry to demonstrate that it is adapted to analyze, both at the qualitative and the quantitative level, and on a high-throughput scale, the changes in the phosphorylation status of many DDR markers that are associated with DNA damage sensing and signaling [28]. A previous study analyzing γH2AX fluorescence intensity using

image cytometry has proven to be quite effective as compared to other methodologies regarding sensitivity, time, and cost per sample while cell number needs was kept minimal [35]. Though H2AX phosphorylation and the activation of other markers such as 53BP1 are evidenced by the formation of foci, we could not easily quantify these foci using this platform, as magnification and resolution are not adapted to this kind of assessment, conversely to fluorescence microscopy. Nevertheless, increase in the number of foci can indirectly be assessed by the global increase in average intensity and we think that such a limitation will be overcome with next generation devices. Here, we report dedicated protocols to assess DNA damage with an extended panel of 11 DDR markers (γH2AX, DNA-PKcs, ATR, ATM, CHK1, CHK2, 53BP1, NBS1, RAD51, P53, and P21), some being evaluated on a multiplexed basis. Our results clearly show the advantage of image cytometry for a rapid analysis of DDR signaling pathways at different levels in a single experiment as exemplified by the re-assessment of the VOX combination (VE-822 and oxaliplatin). They also highlight the advantages of this technology, as very low amounts of antibodies were needed for the detection of each marker, thus drastically reducing running costs as compared to conventional Western blots analyses. Also, image acquisition can be performed in less than one hour for an entire 384-well plate, which is compatible with high throughput screens. We showed for instance that it is possible to compare the effects of two drugs used at five concentrations in triplicate on the 11 individual markers in a single run using only two 384-well plates. Analyzing such a number of markers could also be useful to identify those that are activated by a given drug and to rapidly test its combination with specific inhibitors of these markers to obtain synergistic effects. Furthermore, image cytometry requires quite a reduced number of cells per condition as compared to flow cytometry, which may be of interest for slow-growing cell models such as primary cells. Nevertheless, one should anticipate the need for large computational storage capacity due to the number of images that are generated per experiment. Since image cytometry offers a visual examination of the cells, it is also possible to distinguish a global increase in fluorescence in the whole cell population from a high increase in fluorescence in a small subset of cells, which is impossible to assess using Western blotting. Another advantage of this platform is the possibility to perform multiplexed analyses using up to three DDR markers together with nuclear staining for cell segmentation. Concomitant analyses of these markers within each cell together with the cell cycle status could also be indicative of the heterogeneity of cell response. Indeed, cell treatment with a given drug may activate all the markers of the same pathway in some cells but not in others in which this pathway may not be fully operational, suggesting the existence of potential

resistant clones. While this situation can be easily evidenced by multiplexed analyses of these markers using image cytometry, it cannot be assessed using Western blotting. The example of SN38 in our study is particularly telling as treatment with this Top1 inhibitor induced the phosphorylation of both ATM and ATR in only 62% of HCT116 cells. While this result could be explained by a problem of sensitivity of the method or to a gating issue, it is most likely that heterogeneity of the cell population in terms of cell cycle status or genetic background could translate into a heterogenous DDR, as previously reported [36].

Our study used traditional 2D cell cultures for the evaluation of DNA damage response to anticancer drugs. However, image cytometry could be adapted to other kinds of cell models. In a study by Cribbes *et al*. a 3D model using glioblastoma U87MG cells was used to examine the effects of 14 anticancer drugs in 384-well plates [5]. Size, invasion area of the spheroids, as well as calcein-AM, propidium iodide, Hoechst and caspase 3/7 fluorescence staining to evaluate cell viability were used to generate a score allowing to classify drugs depending on their cytostatic or cytotoxic activity [5]. More recently, Mukundan *et al*. were able to develop a spheroid image cytometry assay using the T47D breast cancer cell line and showed a concentration-dependent reduction of the spheroids following treatment with 6 different anticancer drugs, this effect being correlated with the viability of the cells as measured by calcein-AM and propidium iodide fluorescence staining [37]. These studies demonstrated that image cytometry could be extended to more clinically relevant models such as spheroids, organoids or tissue samples in a high throughput setting. Whether multiplexed evaluation of DNA damage response using our panel of markers could be evaluated using these models needs further investigations.

CONCLUSION

The results of our methodological study confirm the interest in using image cytometry to determine, at high throughput, the effects of a panel of drugs with different mechanism of action, on cell viability and cell death in adherent cancer cell lines of various origins. Our study also provides for the first time valuable methodological guidance for the evaluation of an extended panel of 11 DDR markers to analyze, on a multiplexed-basis, the DNA damage response to various anticancer drugs using image cytometry. Though it is not intended to replace fluorescent microscopy or flow cytometry, our results highlight the time- and cost-

effectiveness of image cytometry as compared to other fluorescence-based methodologies as well as the low amounts of cells that are required for data acquisition.

MATERIALS AND METHODS

Cell culture

Human cancer cell lines from breast (BT-549, SUM159, HCC38, MDA-MB-436), ovarian (OVSAHO and OVCAR-8), prostate (DU 145, PC-3, and 22Rv1) and colon (HCT116) origin were obtained from the TumoroteK bank (SIRIC Montpellier Cancer) and were authenticated by STR (Short-tandem repeat) profiling. Cells were cultured in Dulbecco Modified Eagle Medium (BT-549, MDA-MB-436, DU 145), or RPMI 1640 (HCC38, PC-3, 22Rv1, HCT116) supplemented with 10% fetal bovine serum at 37°C in 5% CO_2 humidified atmosphere. SUM159 were grown in Ham's F-12 medium supplemented with 5% fetal bovine serum, 10 µg/ml insulin, 1 µg/ml hydrocortisone. Cells were routinely tested for mycoplasma contamination using the MycoAlert^{TM} detection kit (Lonza, Basel, Switzerland).

Drugs and reagents

Camptothecin, cisplatin, etoposide, 5-fluorouracile, gemcitabine, PF477736, hydroxyurea (HU), oxaliplatin,, calcein AM, bovine serum albumin (BSA), paraformaldehyde (PFA), Triton-X100, Hoechst 33342, propidium iodide, benzonase and dimethyl sulfoxide (DMSO) were purchased from SIGMA (Saint Quentin Fallavier, France). Olaparib, VE-822 and SN38 were purchased from Selleckchem (Euromedex, Souffelweyersheim, France).

Antibodies

A list of the antibodies used in this study along with the corresponding working dilutions is presented in Table S1. Alexa Fluor 568-conjugated goat anti-rabbit and anti-mouse highly cross-adsorbed secondary antibodies (references A-11036 & A-11031) were purchased from Invitrogen (ThermoFisher Scientific, Courtaboeuf, France).

In vitro cytotoxicity assays

The effects of drugs on cell growth and cell death were measured simultaneously using the Celigo® imaging cytometer as previously described [38]. Briefly, cells were plated in black flat-bottom 96-well plates (Greiner). Twenty four to 48 hours later, exponentially growing

cells were treated with serial dilutions of the different drugs (added in triplicates to the cell media) for additional 72 hours and cells were then stained by adding a mix of Propidium Iodide (PI) and calcein AM (final concentrations of 1 µg/mL and 0.5 µM, respectively). Images were then acquired with the Celigo® imaging cytometer and both PI-positive dead cells and calcein-positive live cells were quantified in each well using the dedicated software. Based on the total number of cells (live + dead), percent growth was calculated for each treated condition in comparison with untreated controls and plotted as a function of drug concentrations to calculate IC_{50} values (drug concentrations required to inhibit the growth of 50% of the cells). Results were the mean ± SEM of ≥ 3 independent experiments.

When cell shape or cell density precluded adequate cell contouring following calcein staining, a dual staining with PI and Hoechst 33342 (final concentrations of 1 and 5 µg/mL, respectively) for 30 min at 37°C was used instead. The number of live cells was then calculated by subtracting the number of dead cells from the number of total cells that was evaluated by Hoechst staining.

Evaluation of DNA Damage Response by immunofluorescence

HCT-116 cells (1,200 cells/well) were plated in black-sided, flat-bottomed 384 well plates (Greiner, Austria). The day after, cells were treated with serial dilutions of the tested drugs 20h and were fixed by an incubation with a solution of 4% PFA-0.1% Triton X-100 for 10 min at room temperature. After blocking with PBS-3% BSA for 1 hour, primary antibodies diluted in PBS-1% BSA were incubated overnight at 4°C with a gentle shaking. For multiplexed assays, 2 or 3 different antibodies could be mixed. Then, cells were washed with PBS-0.2 % Tween 3 times (5, 10, and 15 min) under shaking. Secondary anti-rabbit Alexa Fluor 568 (Invitrogen) or anti-mouse Alexa Fluor 488 antibodies were diluted in PBS-1% BSA (respectively 1/1000 and 1/500) as a mixture and incubated at room temperature for 45 min with gentle shaking in the dark. For the γH2AX antibody that is directly conjugated to the fluorochrome, it was added subsequently to the addition of the secondary antibodies following 3 washes with PBS-0.2% Tween, and were incubated 45min at room temperature in the dark. After these steps, cells were washed 3 more times and were kept in the dark and incubated with 5 µg/mL Hoechst 33342 at 37°C for 30min. Wells were then washed and left in PBS for analysis with the Celigo® Cytometer imaging system.

Statistical analysis

Student's *t*-test were conducted using GraphPad Prism (version 8.1.1) and differences were considered statistically significant for $p<0.01$ (**), and $p<0.001$ (***), respectively.

Supplementary Materials: Figure S1: Representative fluorescent images obtained with OVSAHO and DU145 cells, Figure S2: Dual assessment of the cytotoxic and the cytostatic effects of camptothecin in OVSAHO, PC3, DU145 and HCC38 cells using the Celigo® imaging cytometer, Figure S3: Representative immunofluorescence images that were obtained for each DDR marker using the Celigo® image cytometer, Figure S4 : HCT116 cell response to DNA damaging agents, Figure S5: Time-dependent response of HCT116 cells to DNA damage using γH2AX, pCHK1 and pCHK2 as DDR markers, Figure S6: Validation of the multiplexed analyses of pP53 and P21 DDR markers following DNA damage using the Celigo® image cytometer, Figure S7: Validation of the multiplexed analyses of pATR, pATM and γH2AX DDR markers following DNA damage using the Celigo® image cytometer, Figure S8: Analyses of DDR markers following treatment with the VOX combination using the Celigo® image cytometer, Table S1: List of the primary antibodies used in this study.

Funding: This work was supported by INSERM and the Institut du cancer de Montpellier (ICM) and the SIRIC Montpellier Cancer (Grant INCa_Inserm_DGOS_12553). E. Combès was a recipient of a fellowship from the program Investissement D'avenir of the Labex MabImprove, (Grant ANR-10-LABX-53-01). A.F. Andrade was supported by São Paulo Research Foundation (14/06947-2) and Fondation de France (postdoctoral fellowship).

Acknowledgments: The authors would like to acknowledge the MRI imaging facility, member of the national infrastructure France-BioImaging supported by the French National Research Agency (ANR-10-INBS-04, Investments for the Future) for Celigo® experiments.

Author Contributions: Conceived and designed the experiments: C.G, C.T., N.V-V., M-A.K-H., P.Pa., P.Po. Performed the experiments: A.F.A., E.C., M-A.K-H., N.V-V. Analyzed the data: A.F.A., C.G., E.C., M-A.K-H., M.D.R., N.V-V., P.Po. Contributed reagents/materials/analysis tools: C.G., C.T., P.Pa. Writing – Original Draft preparation: C.G., P.Po. Writing – Review & Editing: C.G., C.T., E.C., M.D.R., N.V-V., P.Pa., P.Po. All authors have read and agreed to the published version of the manuscript.

Conflict of Interest

The authors declare no conflict of interest.

References

1. Stoddart, M.J. Cell Viability Assays: Introduction. *Methods Mol Biol* **2011**, *740*, 1–6
2. Adan, A.; Kiraz, Y.; Baran, Y. Cell Proliferation and Cytotoxicity Assays. *Curr Pharm Biotechnol* **2016**, *17*, 1213–1221
3. Crowley, L.C.; Scott, A.P.; Marfell, B.J.; Boughaba, J.A.; Chojnowski, G.; Waterhouse, N.J. Measuring Cell Death by Propidium Iodide Uptake and Flow Cytometry. *Cold Spring Harb Protoc* **2016**, *2016*
4. Kuksin, D.; Kuksin, C.A.; Qiu, J.; Chan, L.L.-Y. Cellometer Image Cytometry as a Complementary Tool to Flow Cytometry for Verifying Gated Cell Populations. *Anal Biochem* **2016**, *503*, 1–7
5. Cribbes, S.; Kessel, S.; McMenemy, S.; Qiu, J.; Chan, L.L.-Y. A Novel Multiparametric Drug-Scoring Method for High-Throughput Screening of 3D Multicellular Tumor Spheroids Using the Celigo Image Cytometer. *SLAS Discov* **2017**, *22*, 547–557
6. Siqueira-Neto, J.L.; Moon, S.; Jang, J.; Yang, G.; Lee, C.; Moon, H.K.; Chatelain, E.; Genovesio, A.; Cechetto, J.; Freitas-Junior, L.H. An Image-Based High-Content Screening Assay for Compounds Targeting Intracellular Leishmania Donovani Amastigotes in Human Macrophages. *PLoS Negl Trop Dis* **2012**, *6*, e1671
7. Schepers, K.; Pietras, E.M.; Reynaud, D.; Flach, J.; Binnewies, M.; Garg, T.; Wagers, A.J.; Hsiao, E.C.; Passegué, E. Myeloproliferative Neoplasia Remodels the Endosteal Bone Marrow Niche into a Self-Reinforcing Leukemic Niche. *Cell Stem Cell* **2013**, *13*, 285–299
8. Hynes, J.; Carey, C.; Will, Y. Fluorescence-Based Microplate Assays for In Vitro Assessment of Mitochondrial Toxicity, Metabolic Perturbation, and Cellular Oxygenation. *Curr Protoc Toxicol* **2016**, *70*, 2.16.1-2.16.30
9. Franscini, N.; Wuertz, K.; Patocchi-Tenzer, I.; Durner, R.; Boos, N.; Graf-Hausner, U. Development of a Novel Automated Cell Isolation, Expansion, and Characterization Platform. *J Lab Autom* **2011**, *16*, 204–213
10. Bos, A.B.; Duque, J.N.; Bhakta, S.; Farahi, F.; Chirdon, L.A.; Junutula, J.R.; Harms, P.D.; Wong, A.W. Development of a Semi-Automated High Throughput Transient Transfection System. *J Biotechnol* **2014**, *180*, 10–16
11. Amador, C.I.; Stannius, R.O.; Røder, H.L.; Burmølle, M. High-Throughput Screening Alternative to Crystal Violet Biofilm Assay Combining Fluorescence Quantification and Imaging. *J Microbiol Methods* **2021**, *190*, 106343

12. Peña Buttner, W.; Salomo, C.; Sirenko, O.; Hong, D.; Comita, P.; Bogie, S.; Henderson, D.; Olsen, C.; Cromwell, E.F.; Cohen, A. Complex Cell Based Assays with a Novel Imaging Cytometry System and Object Recognition Software 2012.
13. Seranova, E.; Ward, C.; Chipara, M.; Rosenstock, T.R.; Sarkar, S. In Vitro Screening Platforms for Identifying Autophagy Modulators in Mammalian Cells. *Methods Mol Biol* **2019**, *1880*, 389–428
14. Rodrigues Lopes, I.; Silva, R.J.; Caramelo, I.; Eulalio, A.; Mano, M. Shedding Light on MicroRNA Function via Microscopy-Based Screening. *Methods* **2019**, *152*, 55–64
15. Chen, X.; Xun, D.; Zheng, R.; Zhao, L.; Lu, Y.; Huang, J.; Wang, R.; Wang, Y. Deep-Learning-Assisted Assessment of DNA Damage Based on Foci Images and Its Application in High-Content Screening of Lead Compounds. *Anal Chem* **2020**, *92*, 14267–14277
16. Combès, E.; Andrade, A.F.; Tosi, D.; Michaud, H.-A.; Coquel, F.; Garambois, V.; Desigaud, D.; Jarlier, M.; Coquelle, A.; Pasero, P.; et al. Inhibition of Ataxia-Telangiectasia Mutated and RAD3-Related (ATR) Overcomes Oxaliplatin Resistance and Promotes Antitumor Immunity in Colorectal Cancer. *Cancer Res* **2019**, *79*, 2933–2946
17. Hsiang, Y.H.; Hertzberg, R.; Hecht, S.; Liu, L.F. Camptothecin Induces Protein-Linked DNA Breaks via Mammalian DNA Topoisomerase I. *J Biol Chem* **1985**, *260*, 14873–14878
18. Furuta, T.; Hayward, R.L.; Meng, L.-H.; Takemura, H.; Aune, G.J.; Bonner, W.M.; Aladjem, M.I.; Kohn, K.W.; Pommier, Y. P21CDKN1A Allows the Repair of Replication-Mediated DNA Double-Strand Breaks Induced by Topoisomerase I and Is Inactivated by the Checkpoint Kinase Inhibitor 7-Hydroxystaurosporine. *Oncogene* **2006**, *25*, 2839–2849
19. Chen, J. Ataxia Telangiectasia-Related Protein Is Involved in the Phosphorylation of BRCA1 Following Deoxyribonucleic Acid Damage. *Cancer Res* **2000**, *60*, 5037–5039.
20. Shoemaker, R.H. The NCI60 Human Tumour Cell Line Anticancer Drug Screen. *Nat Rev Cancer* **2006**, *6*, 813–823
21. Kim, J.S.; Hur, D.; Hwang, J.K.; Chung, C.; Chang, J.K. Ongoing Development of Image Cytometers. *Bioanalysis* **2010**, *2*, 1755–1765
22. Chan, L.L.-Y.; McCulley, K.J.; Kessel, S.L. Assessment of Cell Viability with Single-, Dual-, and Multi-Staining Methods Using Image Cytometry. *Methods Mol Biol* **2017**, *1601*, 27–41

23. Wang, Z. Cell Segmentation for Image Cytometry: Advances, Insufficiencies, and Challenges. *Cytometry A* **2019**, *95*, 708–711
24. Longley, D.B.; Harkin, D.P.; Johnston, P.G. 5-Fluorouracil: Mechanisms of Action and Clinical Strategies. *Nat Rev Cancer* **2003**, *3*, 330–338
25. Harper, J.W.; Elledge, S.J. The DNA Damage Response: Ten Years After. *Mol Cell* **2007**, *28*, 739–745
26. Jackson, S.P.; Bartek, J. The DNA-Damage Response in Human Biology and Disease. *Nature* **2009**, *461*, 1071–1078
27. Rogakou, E.P.; Pilch, D.R.; Orr, A.H.; Ivanova, V.S.; Bonner, W.M. DNA Double-Stranded Breaks Induce Histone H2AX Phosphorylation on Serine 139. *J Biol Chem* **1998**, *273*, 5858–5868
28. Bonner, W.M.; Redon, C.E.; Dickey, J.S.; Nakamura, A.J.; Sedelnikova, O.A.; Solier, S.; Pommier, Y. GammaH2AX and Cancer. *Nat Rev Cancer* **2008**, *8*, 957–967
29. Lanz, M.C.; Dibitetto, D.; Smolka, M.B. DNA Damage Kinase Signaling: Checkpoint and Repair at 30 Years. *EMBO J* **2019**, *38*, e101801
30. Darzynkiewicz, Z.; Traganos, F.; Zhao, H.; Halicka, H.D.; Skommer, J.; Wlodkowic, D. Analysis of Individual Molecular Events of DNA Damage Response by Flow- and Image-Assisted Cytometry. *Methods Cell Biol* **2011**, *103*, 115–147
31. Mistrik, M.; Oplustilova, L.; Lukas, J.; Bartek, J. Low-Dose DNA Damage and Replication Stress Responses Quantified by Optimized Automated Single-Cell Image Analysis. *Cell Cycle* **2009**, *8*, 2592–2599
32. Wilsker, D.F.; Barrett, A.M.; Dull, A.B.; Lawrence, S.M.; Hollingshead, M.G.; Chen, A.; Kummar, S.; Parchment, R.E.; Doroshow, J.H.; Kinders, R.J. Evaluation of Pharmacodynamic Responses to Cancer Therapeutic Agents Using DNA Damage Markers. *Clin Cancer Res* **2019**, *25*, 3084–3095
33. Forment, J.V.; Walker, R.V.; Jackson, S.P. A High-Throughput, Flow Cytometry-Based Method to Quantify DNA-End Resection in Mammalian Cells. *Cytometry A* **2012**, *81*, 922–928
34. Forment, J.V.; Jackson, S.P. A Flow Cytometry-Based Method to Simplify the Analysis and Quantification of Protein Association to Chromatin in Mammalian Cells. *Nat Protoc* **2015**, *10*, 1297–1307
35. Fowler, T.L.; Bailey, A.M.; Bednarz, B.P.; Kimple, R.J. High-Throughput Detection of DNA Double-Strand Breaks Using Image Cytometry. *Biotechniques* **2015**, *58*, 37–39

36. Ben-David, U.; Siranosian, B.; Ha, G.; Tang, H.; Oren, Y.; Hinohara, K.; Strathdee, C.A.; Dempster, J.; Lyons, N.J.; Burns, R.; et al. Genetic and Transcriptional Evolution Alters Cancer Cell Line Drug Response. *Nature* **2018**, *560*, 325–330
37. Mukundan, S.; Bell, J.; Teryek, M.; Hernandez, C.; Love, A.C.; Parekkadan, B.; Chan, L.L.-Y. Automated Assessment of Cancer Drug Efficacy On Breast Tumor Spheroids in Aggrewell^{TM}400 Plates Using Image Cytometry. *J Fluoresc* **2022**, *32*, 521–531
38. Kessel, S.; Cribbes, S.; Déry, O.; Kuksin, D.; Sincoff, E.; Qiu, J.; Chan, L.L.-Y. High-Throughput 3D Tumor Spheroid Screening Method for Cancer Drug Discovery Using Celigo Image Cytometry. *SLAS Technol* **2017**, *22*, 454–465